Scientific Report

SOURCE DATA | TRANSPARENT PROCESS

EMBO reports

Selenoprotein T is a novel OST subunit that regulates UPR signaling and hormone secretion

Abdallah Hamieh[1,2], Dorthe Cartier[1,2], Houssni Abid[1,2], André Calas[3], Carole Burel[2,4], Christine Bucharles[1,2], Cedric Jehan[1,2], Luca Grumolato[1,2], Marc Landry[3], Patrice Lerouge[2,4], Youssef Anouar[1,2] & Isabelle Lihrmann[1,2,*]

Abstract

Selenoprotein T (SelT) is a recently characterized thioredoxin-like protein whose expression is very high during development, but is confined to endocrine tissues in adulthood where its function is unknown. We report here that SelT is required for adaptation to the stressful conditions of high hormone level production in endocrine cells. Using immunofluorescence and TEM immunogold approaches, we find that SelT is expressed at the endoplasmic reticulum membrane in all hormone-producing pituitary cell types. SelT knockdown in corticotrope cells promotes unfolded protein response (UPR) and ER stress and lowers endoplasmic reticulum-associated protein degradation (ERAD) and hormone production. Using a screen in yeast for SelT-membrane protein interactions, we sort keratinocyte-associated protein 2 (KCP2), a subunit of the protein complex oligosaccharyltransferase (OST). In fact, SelT interacts not only with KCP2 but also with other subunits of the A-type OST complex which are depleted after SelT knockdown leading to POMC N-glycosylation defects. This study identifies SelT as a novel subunit of the A-type OST complex, indispensable for its integrity and for ER homeostasis, and exerting a pivotal adaptive function that allows endocrine cells to properly achieve the maturation and secretion of hormones.

Keywords ER stress; KCP2; N-glycosylation; oligosaccharyl transferase; pituitary

Subject Categories Membrane & Intracellular Transport; Physiology; Post-translational Modifications, Proteolysis & Proteomics

DOI 10.15252/embr.201643504 | Received 13 October 2016 | Revised 4 August 2017 | Accepted 9 August 2017 | Published online 19 September 2017

EMBO Reports (2017) 18: 1935–1946

Introduction

A particular class of ER proteins named selenoproteins incorporates the essential micronutrient selenium (Se) as the 21st amino acid selenocysteine (Sec; U) through a highly regulated mechanism requiring specific intracellular limiting factors and a dedicated tRNA ($tRNA_{Sec}$) for the Sec residue [1–4]. Twenty-five selenoproteins were identified in the human genome, which localize to various cellular compartments including the ER and are involved in diverse biological processes [2–6]. Among them, glutathione peroxydases and thioredoxin reductases control redox homeostasis, while iodothyronine deiodinases are important in the activation and deactivation of thyroid hormones [4,7–9], but the role of many selenoproteins is still elusive. The absence of all selenoproteins obtained by suppression of the Trsp gene encoding the $tRNA_{Sec}$ results in early death of embryos due to abnormal growth of the skeleton and cartilage [10]. Moreover, selenoprotein deficiency has been associated with cerebral and cardiovascular dysfunction and cancer [11–13].

Selenoprotein T (SelT) is a thioredoxin-like enzyme with a CXXU motif, which is up-regulated during neuroendocrine cell differentiation [14,15]. It is widely expressed during development [16,17], and its genetic ablation in mice results in embryonic lethality before embryonic day (E)8 [15]. SelT gene expression is temporally tightly regulated since its levels decline in most adult tissues, except in endocrine glands such as pituitary, pancreas, testis, and thyroid where they remain elevated [16,17]. Akin to other selenoproteins such as SelN, SelM, and SelK, SelT may contribute to the regulation of Ca^{2+} homeostasis in the ER [5,14,18,19].

In the present study, we sought to decipher the precise function of SelT in endocrine cells such as pituitary cells. Indeed, the anterior pituitary gland contains several hormone-producing cell types, which can markedly remodel their metabolism in response to changes in endocrine needs of the organism. It plays a major role in mammalian physiology by regulating growth, metabolism, lactation, stress, and reproduction [20]. We show here that, in endocrine cells, SelT is a novel subunit of the A-type oligosaccharyltransferase (OST) complex indispensable for its integrity, for ER homeostasis and glycoprotein hormone secretion.

1 Neuronal and Neuroendocrine Differentiation and Communication Laboratory, Rouen-Normandie University, UNIROUEN, Inserm, U1239, Mont-Saint-Aignan, France
2 Institute for Research and Innovation in Biomedicine, Rouen, France
3 Interdisciplinary Institute for Neuroscience, CNRS UMR 5297, University of Bordeaux, Bordeaux, France
4 Glyco-MEV Laboratory, Rouen-Normandie University, UNIROUEN, Mont-Saint-Aignan, France
*Corresponding author. Tel: +(33)235 14 6626; Fax: +(33) 235 14 6946; E-mail: isabelle.lihrmann@univ-rouen.fr

Results and Discussion

Alteration of adrenocoticotropic hormone secretion in SelT-deficient corticotrope cells

In line with our previous studies [16,17], SelT immunoreactivity was detected in the anterior pituitary, within all endocrine cells, including lactotrope, gonadotrope, thyreotrope, corticotrope, and somatotrope cells (Fig 1A), albeit at a great inter-cell variability also evidenced at the ultrastructural level using a high-resolution silver-amplified immunogold TEM analysis (Fig 1B$_{a,b}$). SelT was observed at the ER membrane (Fig 1B$_{c,d}$), and occasionally at the plasma membrane (Fig 1B$_{d}$), but not in secretory granules (Fig 1B$_{e,f}$) or mitochondria (Fig 1B$_{g}$). In the corticotrope AtT20 cells, which produce and release in a corticotropin-releasing factor (CRF)-dependent manner the multivalent prohormone proopiomelanocortin (POMC) and its processing product adrenocorticotropic hormone (ACTH) (Fig 1C), SelT protein was also readily detected (Fig 1D). Immunofluorescence images showed that SelT staining in these cells largely, although not exclusively, colocalizes with the staining of the ER (Fig 1E), consistent with our TEM data (Fig 1B) and with other results indicating the presence of SelT in ER, and also in Golgi [14,21]. The deletion of a SelT region (positions 85–103 and 125–144 of NP_001035486.2) with two predicted (TMPRED software) transmembrane helices led to a diffuse relocation of the protein in the cytosol (Fig 1F), indicating that this domain is necessary and sufficient to retain SelT in the ER compartment. Treatment by CRF (100 nM; 24 h) increased SelT mRNA levels (2.6-fold; Fig 1G) and ACTH secretion (1.5-fold; Fig 1H) in AtT20 cells. In contrast, SelT depletion led to a reduction of basal ACTH secretion and abrogation of the CRF-induced ACTH secretion (Fig 1H), associated with a 45–55% reduction in ACTH content in control and CRF-stimulated cells (Fig 1I). Altogether, these data indicate that SelT is essential for basal- and stimulated-hormone production, in agreement with our previous work showing insulin production deficiency in SelT-insKO mice [16].

SelT is essential to maintain ER homeostasis

In addition to hormone production defect, SelT-deficient cells also showed an ER dilatation, visualized by ER-DsRed distribution, like cells exposed to a non-permissive temperature (39°C) (Fig 2A) [22]. SelT knockdown also significantly increased CHOP (twofold) and BIP (fourfold) levels (Fig 2B), two of the best studied proteins induced by ER stress [23]. Activated UPR sensors send information to the nucleus to regulate the transcription of many genes to resolve

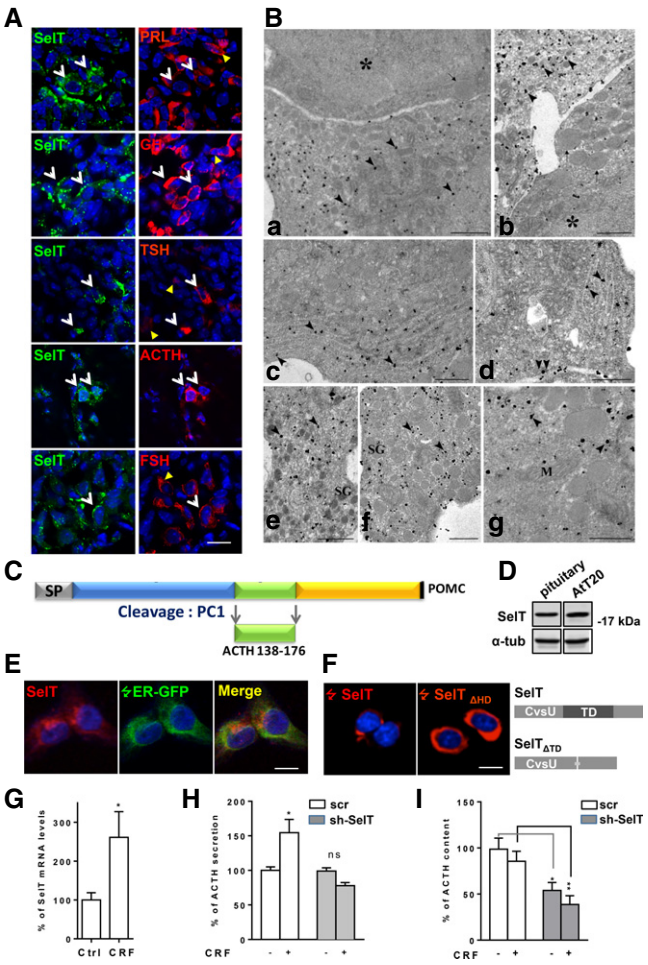

Figure 1. Alteration of adrenocoticotropic hormone secretion in SelT-deficient corticotrope cells.

A Double immunostaining of pituitary sections for SelT (green) and hormones (red). Nuclei were labeled with DAPI (blue). Each hormone positive cell type expresses SelT (white arrows), but not all cells (yellow arrows) contain SelT. Scale bar, 12 μm.

B TEM images of adenohypophysis showing SelT ultrastructural distribution. Sections were treated with SelT antibody and visualized with silver-enhanced, gold-labeled secondary antibodies. (a, b) Heavily labeled cells revealed by silver grains (arrowheads) are adjacent to weakly labeled ones (asterisks) characterized by distinct secretory content (arrows). (c, d) Immunopositive cells display silver grains on the ER membrane (arrowheads) and at the plasma membrane (double arrowhead in d). (e–g) Labeling (arrowheads) is restricted to cytoplasmic domains excluding secretory granules (SG) and mitochondria (M). Scale bar, 0.5 μm.

C Schematic representation of POMC, which generates ACTH after cleavage by PC1 in AtT20 cells.

D Western blot analysis of SelT expression in mouse pituitary and pituitary corticotrope AtT20 cells.

E Immunohistochemical analysis of Myc-SelT (red) intracellular distribution in AtT20 cells; the ER compartment was labeled with transiently expressed ER-GFP (green). DAPI was used to stain the nuclei. Scale bar, 12 μm.

F A Myc-SelT variant carrying a deletion of the hydrophobic domains (SelTΔTD) showed relocation from the ER (left) to the cytosol (right). Scale bar, 12 μm.

G qRT–PCR analysis of SelT expression in the presence of CRF (100 nM, 24 h) in scr shRNA-transduced AtT20 cells. Asterisks denote statistical significance. Each value is the mean ± SEM (n = 7, *P < 0.05; Mann–Whitney test).

H Analysis of ACTH concentration in cell culture supernatants by ACTH ELISA assay. Scr and SelT shRNA-transduced AtT20 cells were treated with 100 nM of CRF for 24 h. Data are expressed as percentage of control (untreated cells; set to 100). Each value is the mean ± SEM (n = 3, *P < 0.05; Mann–Whitney test).

I Analysis of scr and SelT shRNA-transduced AtT20 cells content by ACTH ELISA assay. Data are expressed as percentage of control (untreated AtT20 cells; set to 100). Each value is the mean ± SEM (n = 3; *P < 0.05; **P < 0.01, two-way ANOVA).

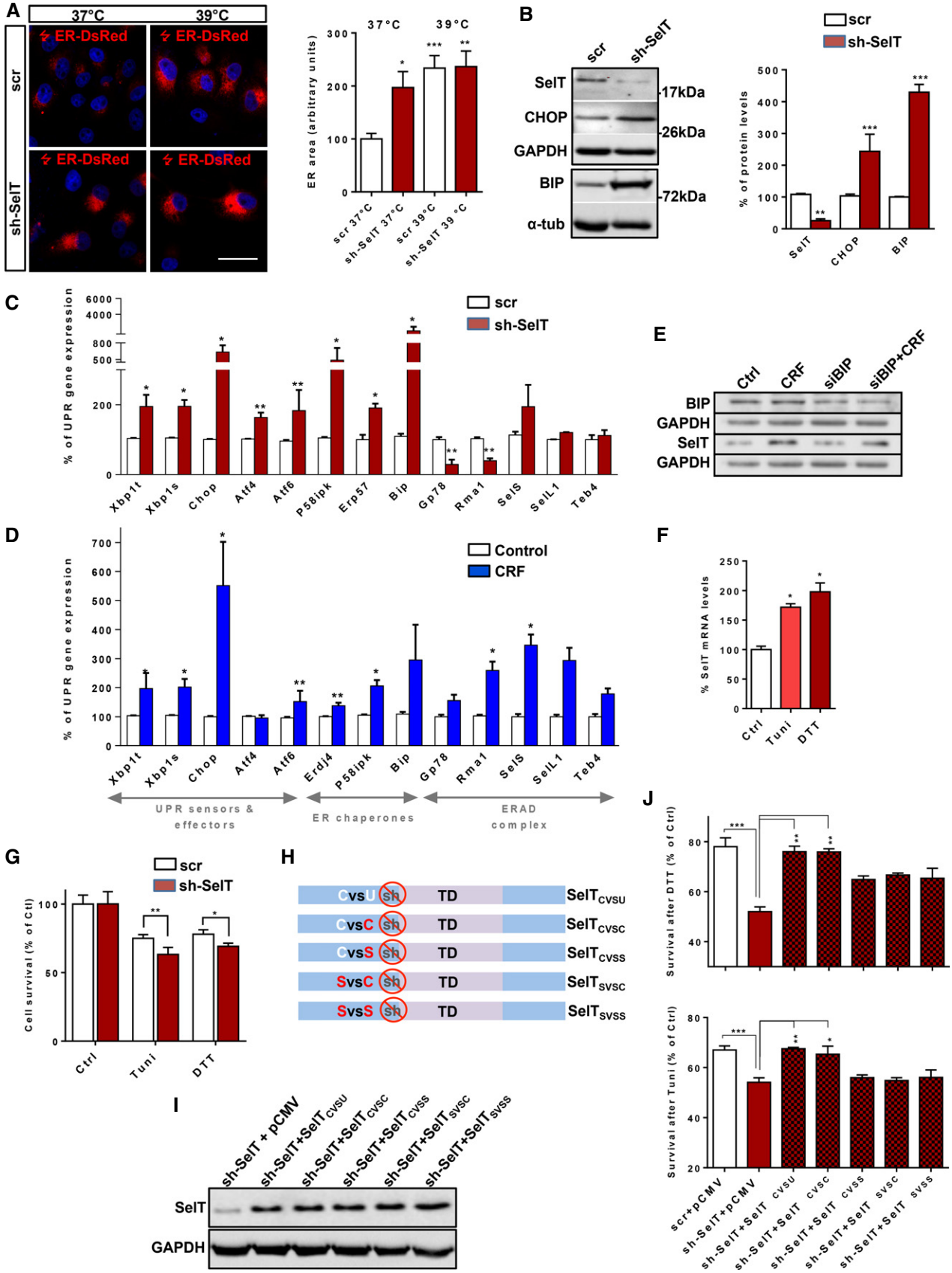

Figure 2.

Figure 2. SelT is required for ER homeostasis.

A Confocal imaging of ER in scr and SelT shRNA-transduced AtT20 cells transfected with ER-DsRed vector (red) and grown at 37 or 39°C for 16 h. Nuclei were labeled with DAPI (blue). The number of red pixels per cell, representing the ER area, was measured using the ImageJ software. Data are expressed as percentage of control (scr transduced cells grown at 37°C; set to 100). Scale bar, 25 μm. Each value is the mean ± SEM (n = 8; *P < 0.05; **P < 0.01; ***P < 0.0001; Mann–Whitney test).

B Western blot analysis of ER stress markers, CHOP and BIP, in scr and SelT shRNA-transduced AtT20 cells. GAPDH was used as an internal loading control. Relative protein levels were measured with the Image Lab software (Bio-Rad) and expressed as percentage of control (scr set to 100). Each value is the mean ± SEM ($n \geq 3$; **P < 0.01; ***P < 0.001; Mann–Whitney test).

C qRT–PCR analysis of the expression of ER stress-responsive genes in scr and SelT shRNA-transduced AtT20 cells. Data are expressed as percentage of control (scr set to 100). Each value is the mean ± SEM ($n \geq 3$; *P < 0.05; **P < 0.01; Mann–Whitney test).

D qRT–PCR analysis of the expression of ER stress-responsive genes in scr and CRF (100 nM, 24 h)-treated scr cells. Each value is the mean ± SEM ($n \geq 2$, *P < 0.05; **P < 0.01; Mann–Whitney test).

E Western blot analysis of SelT and BIP expression in AtT20 cells after *Bip* knock down in basal conditions and after CRF (100 nM) treatment for 24 h.

F qRT–PCR analysis of SelT expression in the presence of two ER stressors, Tuni (1 μg/ml) and DTT (100 μM) for 6 h in wild-type (scr) AtT20 cells (Ctrl set to 100). Each value is the mean ± SEM (n = 3–5; *P < 0.01; one-way-ANOVA).

G Comparison of the viability of scr and SelT shRNA-transduced AtT20 cells treated with Tuni (1 μg/ml) or DTT (100 μM) for 24 h. Data are expressed as percentage of control (scr set to 100). Each value is the mean ± SEM (n = 5; *P < 0.01; **P < 0.01; one-way-ANOVA).

H Schematic representation of shRNA-resistant forms of SelT, native, or carrying a series of substitutions in the CSVU motif, designed to rescue the SelT shRNA effect.

I Detection of recombinant SelT mutants in SelT shRNA-expressing AtT20 cells by Western blot analysis.

J Viability analysis of scr and SelT shRNA-transduced AtT20 cells rescued with a series of mutants described in (H), in ER stress conditions using 1 μg/ml Tuni (top panel) or 100 μM DTT (bottom panel) for 24 h. Each value is the mean ± SEM ($n \geq 5$; *P < 0.05; **P < 0.01; ***P < 0.001; Mann–Whitney test).

Source data are available online for this figure.

protein misfolding and restore an efficient protein-folding environment. Indeed, the UPR sensor gene Atf6 and the effector genes ChoP and Atf4 were significantly activated in shSelT-treated cells. Total Xbp1 mRNA levels were also increased by ~2-fold, as was the spliced form of Xbp1 mRNA encoding the active form of XBP1. Among ER chaperones, *Bip* mRNA was tremendously increased (Fig 2C). Noteworthy, UPR activation in AtT20 cells was also observed upon CRF treatment (100 nM, 24 h) (Fig 2D), consistent with the notion that in tissues with intense secretory activity, a physiological UPR is activated to prevent ER stress [24–28]. Thus, in endocrine cells, SelT could be instrumental for the protection against ER stress generated during stimulation of hormone production.

We next investigated whether SelT expression is controlled by UPR activation, using a siRNA against *Bip/Grp78* whose suppression activates UPR signaling [29,30]. Neither basal nor CRF-induced SelT expression was altered by BIP knockdown (Fig 2E), thus ruling out this possibility. In contrast, tunicamycin (Tuni; 1 μg/ml) and dithiothreitol (DTT; 100 μM), two commonly used ER stressors, increased SelT mRNA levels (Tuni, 1.6-fold; DTT, twofold) after 6-h treatment (Fig 2F). Furthermore, SelT depletion caused an increase in the sensitivity to these ER stress inducers (Fig 2G) since cell viability was reduced by 25 and 20% in control cells, and by 37 and 31% in SelT-depleted cells, after 24 h treatment by Tuni or DTT, respectively. Control rescue experiments were performed by expressing various shRNA-resistant forms of SelT mRNA, some carrying mutations in the redox CXXU center, but all containing the SECIS sequence necessary to direct incorporation of the Sec residue at the stop codon (Fig 2H) and produce full-length proteins in AtT20 cells (Fig 2I). Recombinant $SelT_{CVSU}$ and $SelT_{CVSC}$, but not mutants with Cys or Sec disruption in the redox center, restored survival of AtT20 cells exposed to both ER stressors (Fig 2J). Of note, SelT knockdown did not alter survival of AtT20 cells in basal condition, suggesting that SelT activity is essential for adaptation to the stressful conditions of high hormone level production, but not for survival of quiescent endocrine cells. The variability of SelT levels that we observed within the same anterior pituitary cell populations may thus reflect the existence of discrete cell subpopulations which differ in their molecular signaling and secretory activity in order to finely adjust their dynamic response to the specific hormonal requirements [31,32]. Overall, these data suggest that SelT redox function is pivotal to maintain ER homeostasis and cell survival when pharmacological (Tuni, DTT) or physiological (CRF) disruption of ER folding events lead to the buildup of unfolded polypeptides in the ER lumen and thus to ER stress [33].

SelT-depleted cells are defective in ER-associated degradation of unfolded proteins

Although ERAD gene activation in SelT-depleted cells was expected as a consequence of IRE1α and ATF6 activation [34], a drastic decrease of Gp78 (72%) and Rma1 (76%) gene expression was found (Fig 2C), suggesting that misfolded proteins may accumulate in the ER after SelT knockdown due to ERAD dysfunction. To address this issue, we monitored in the presence of cycloheximide the degradation of the green fluorescent protein (GFP)-tagged secretion-incompetent variant mutant of human α1-antitrypsin (Null Hong Kong mutant or NHK), which does not fold properly and is targeted for degradation by the proteasome [35]. NHK-GFP was rapidly degraded in cells transduced with the control scrambled (scr) shRNA, that is, 20% was left at 1.5 h of cycloheximide treatment and less than 10% at 3-h treatment. However, this degradation was delayed in SelT-depleted cells, where 100% was left at 1.5 h of cycloheximide treatment and 40% at 3-h treatment (Fig 3A and B), supporting the notion of a failure of ERAD to eliminate misfolded proteins in SelT-deficient corticotrope cells, although a possible proteasome deficiency could be also involved. The latter hypothesis remains to be explored.

SelT interacts with KCP2 and stabilizes A-type OST subunits

ER membrane is known as a privileged site to recruit proteins into complexes, and several membrane-bound selenoproteins like selenoproteins S, K, and N have been shown to be associated with

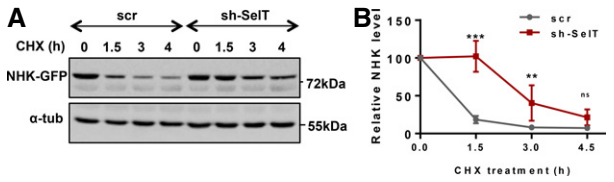

Figure 3. SelT deficiency slows down ER-associated protein degradation.

A Scr and SelT shRNA-transduced AtT20 cells were transiently transfected with an expression plasmid encoding the GFP-tagged Hong Kong variant of mutant α1-antitrypsin (NHK-GFP). AtT20 cells were pulse-chased for the indicated time and analyzed by Western blot analysis using an anti-GFP antibody. α-tubulin was used as an internal loading control.

B Quantification of GFP-tagged NHK degradation rate in (A). Relative NHK-GFP levels were calculated by dividing the normalized GFP signals in cells after 1.5, 3, and 4.5 h of cycloheximide (CHX) treatment with that of untreated cells (untreated cells set to 100). Each value is the mean ± SEM (n = 4; $^{**}P < 0.01$; $^{***}P < 0.001$; two-way ANOVA test).

Source data are available online for this figure.

protein complexes [18,36–39]. In order to identify SelT interactants, we used a modified split-ubiquitin system for *in vivo* detection of interactions between transmembrane proteins in yeast. The full-length rat SelT, in which the Sec was converted to a Cys because yeast does not have the selenoprotein synthesis machinery, was used as bait. Four clones from different colonies were sorted, all containing the full-length cDNA encoding keratinocyte-associated protein 2 (alias KCP2; Krtcap2; GID:142382643). This ER 14-kDa protein comprising 136-aa and three transmembrane spans (Fig 4A and B) was characterized from solubilized actively engaged ribosomes within the OST complex [40–42]. Noteworthy, KCP2 is abundant in active secretory tissues [43]. Co-immunoprecipitation (co-IP) experiments showed that endogenous KCP2 coprecipitates with endogenous SelT and *vice versa* in AtT20 cells (Fig 4C), supporting the specific interaction between SelT and KCP2 in these cells. The OST complex catalyzes the *en bloc* transfer of preassembled high-mannose oligosaccharides onto asparagine residues present within the N-X-T/S motif of nascent polypeptides entering the lumen of the rough ER, a process essential for the productive folding, stability, trafficking, ligand-binding, and interaction with extracellular matrix of many secretory and membrane proteins [44–47]. Two OST isoforms exist, the A and B types, which are distinguished by the presence of STT3A or STT3B catalytic subunits [48], and have complementary roles to optimize protein N-glycosylation. The A-type catalyzes the cotranslational N-glycosylation of nascent proteins, while the B type performs the post-translational N-glycosylation of particular sequons [46]. A series of five non-catalytic subunits are also present in each complex including ribophorin I, ribophorin II, OST48, DAD1, and OST4, as well as isoform-specific subunits, that is, Tusc3, MagT1, KCP2, and DC2 [49]. Co-IP studies revealed that, in non-denaturing conditions, in addition to KCP2, SelT also associates with STT3A and OST48 but not with STT3B (Fig 4D), in line with previous data showing that KCP2 is a preferential subunit of the A-type OST complex [41,42]. SelT and KCP2 interactions were further validated by immunofluorescence data showing that SelT and KCP2 signals overlap in AtT20 cells (Fig 4E). In addition, both SelT and KCP2 were detected in microsomal membranes (Fig 4F), although SelT was not systematically present, suggesting that it may be associated with the membrane under certain conditions, or that its association with the membrane is weak [39]. A treatment with Tuni did not change the migration pattern of SelT (Fig 4G), ruling out the possibility that SelT is transiently associated with OST to be N-glycosylated.

We next tested the possibility that SelT is necessary for the assembly or the stability of the A-type OST complex, as shown previously for other subunits [40,46,50]. We found that stable expression of a SelT shRNA in AtT20 cells, which decreased SelT protein content by 76% as compared to cells expressing the scr shRNA (Fig 4H), also reduces KCP2, STT3A, OST48, but not STT3B, protein levels (Fig 4I), while their respective mRNA levels were unaffected (Fig 4J). Similarly, the levels of the β subunit of the ER resident Sec61 translocon, which often copurifies with OST, were

Figure 4. SelT interacts with KCP2 and stabilizes A-type OST subunits.

A ER membrane topology of KCP2 (generated with Protter http://wlab.ethz.ch/protter/start/).

B Schematic representation of the four KCP2-related prey fragments found to interact with SelT in the yeast two-hybrid screen. In green, lumenal domains; in orange, cytoplasmic domains.

C Co-immunoprecipitation analysis of SelT and KCP2 interactions in AtT20 cells. Proteins interacting with endogenous SelT and KCP2 were immunoprecipitated with SelT and KCP2 antibodies, respectively, and analyzed by Western blot. IgG, irrelevant antibody.

D Co-immunoprecipitation analysis of SelT and STT3A, STT3B, and OST48 subunit interactions in AtT20 cells. Proteins interacting with endogenous SelT, STT3A, STT3B, OST48, and KCP2 were immunoprecipitated with SelT, STT3A, STT3B, OST48, and KCP2 antibodies, respectively, and analyzed by Western blot. IgG, irrelevant antibody.

E Dual immunofluorescence staining showing SelT (green) and KCP2 (red) colocalization in AtT20 cells. Scale bar, 10 μm.

F Western blot detection of SelT and KCP2 in AtT20 cell microsomal preparation. SelT and KCP2 were detected in whole AtT20 cell lysate (Ctrl) and in the microsomal (Mic) fraction.

G Western blot analysis of SelT expression in control AtT20 cells in the presence or absence of Tuni (1 μg/ml). GAPDH was used as an internal loading control.

H Western blot analysis of SelT expression in scr and SelT shRNA-transduced AtT20 cells. α-tubulin antibody was used as a loading control. Data are expressed as percentage of control (scr; set to 100). Each value is the mean ± SEM (n = 5; $^{**}P < 0.01$; t-test).

I KCP2, STT3A, OST48, STT3B, and Sec61β protein levels were analyzed by Western blot in scr and SelT shRNA-transduced AtT20 cells. GAPDH was used as an internal loading control. Relative protein levels were measured with the Image Lab software (Bio-Rad) and expressed as percentage of control (scr; set to 100) (right panel). Each value is the mean ± SEM ($n \geq 3$; $^{*}P < 0.05$; $^{**}P < 0.01$; Mann–Whitney test).

J qRT–PCR analysis of KCP2, STT3A, and OST48 mRNA levels in scr and SelT shRNA-transduced AtT20 cells. Data are expressed as percentage of control (scr; set to 100). Values are expressed as mean ± SEM ($n \geq 3$; Mann–Whitney test).

K KCP2, SelT, STT3A, and OST48 protein levels were analyzed by Western blot in scr and KCP2 siRNA-tranduced AtT20 cells. α-tubulin was used as an internal loading control. Relative protein levels were measured with the Image Lab software (Bio-Rad) and expressed as percentage of control (scr; set to 100) (right panel). Each value is the mean ± SEM ($n \geq 3$; $^{*}P < 0.05$; Mann–Whitney test).

Source data are available online for this figure.

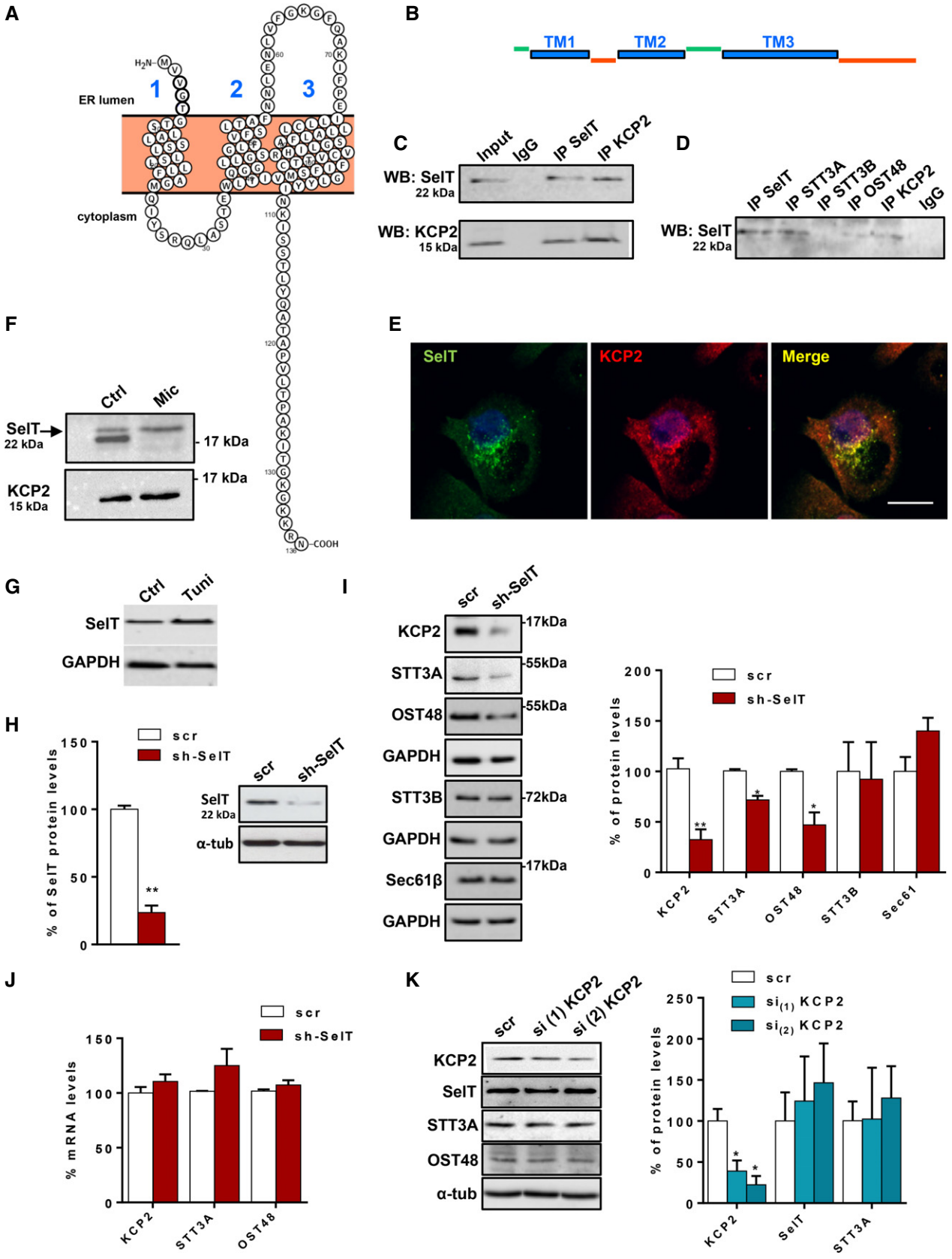

Figure 4.

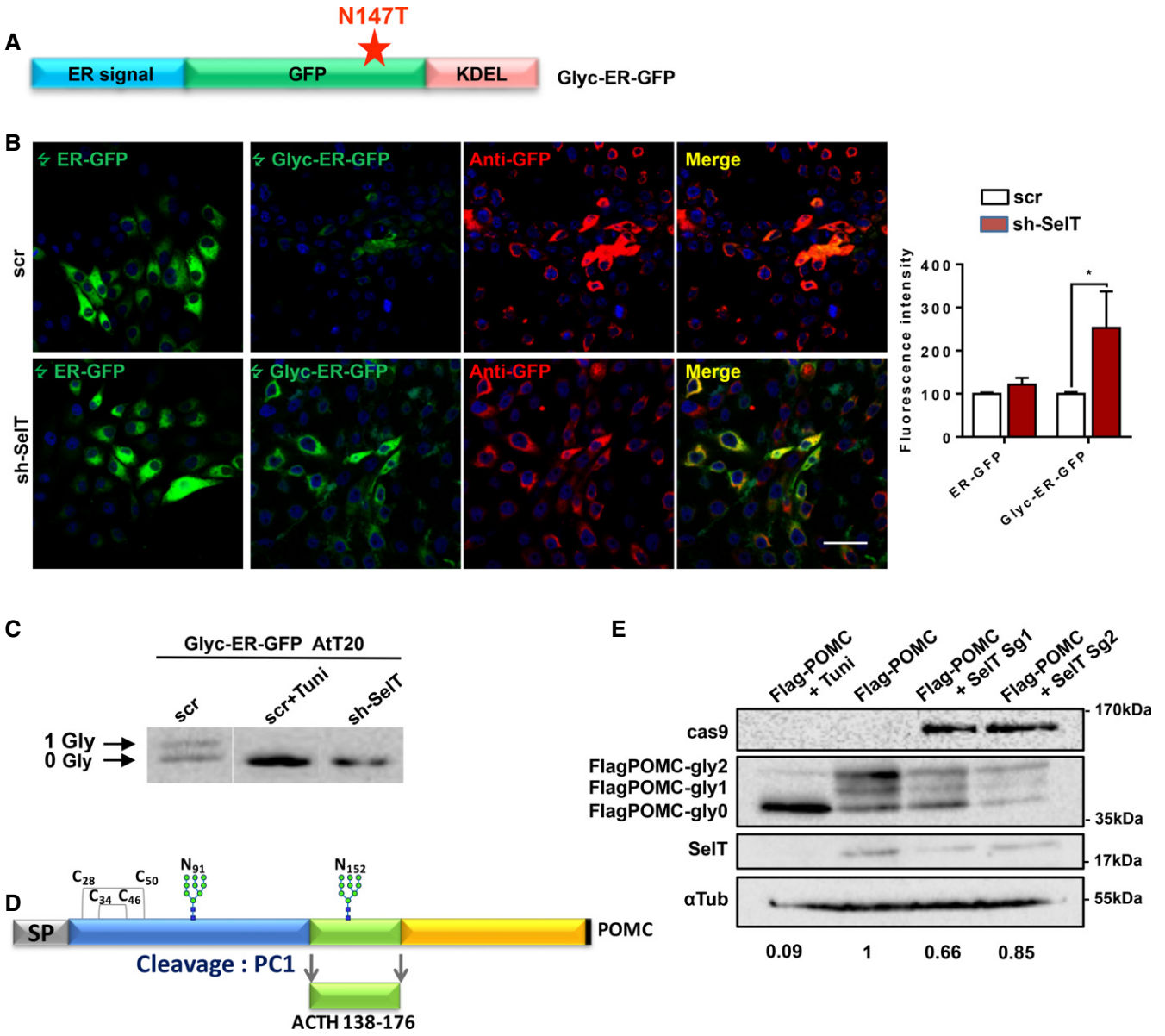

Figure 5. SelT depletion perturbs N-glycosylation.

A Schematic representation of the Glyc-ER-GFP construct. Red star: Mutation N147T inserted; ER signal: calreticulin ER signal sequence; KDEL: ER retention sequence (modified from Losfeld *et al*, 2012).

B Scr and SelT shRNA-tranduced AtT20 cells were transiently transfected with ER-GFP and Glyc-ER-GFP (green). Glyc-ER-GFP transfected cells were immunolabeled by anti-GFP (red). For Glyc-ER-GFP quantification, the number of green and red pixels was measured using the ImageJ software. Number of green pixels was normalized to the number of red pixels in each condition. Nuclei were labeled with DAPI (blue). Scale bar, 50 μm. Data are expressed as percentage of control (scr set to 100). Each value is the mean ± SEM (n = 4; *P < 0.05; Mann–Whitney test).

C Western blot analysis of expression of glycosylated or non-glycosylated GFP in scr and SelT shRNA-tranduced AtT20 cells transiently transfected by Glyc-ER-GFP and treated or not with 1 μg/ml of Tuni.

D Diagram of POMC precursor showing the disulfide bridges and the N-glycosylation sequons.

E Western blot analysis of glycoforms of exogenous Flag-POMC in AtT20 cells, after SelT gene disruption using CRISPR Cas9 technology, or in the presence of Tuni. Glycoforms in the cells invalidated for the SelT gene by CRISPR Cas9 technology were expressed relative to the normalized signal in non-invalidated cells. Quantified values below gel lanes are for the displayed image, that is, representative of two or more experiments.

Source data are available online for this figure.

not altered upon SelT depletion or when OST subunits are depleted [46,51] (Fig 4I). As an additional control, KCP2 deficiency did not affect SelT or other A-type OST subunits (Fig 4K), as shown previously [40]. Altogether, these data demonstrate that SelT is required to maintain high levels of the A-type OST complex. Its high expression in adult tissues with high glycoprotein secretion activity

[16,17] resembles that of both KCP2 and STT3A and less that of STT3B [41,43], supporting the idea that SelT associates with OST to contribute to its integrity preferentially in endocrine tissues when hormone demand is high. Whether the redox site, which is critical for other selenoproteins to form complexes [18,36], is also necessary for SelT assembly with the A-type OST and/or its stabilization in endocrine cells remains to be determined.

SelT impacts protein N-glycosylation

Reduction of the expression of several A-type OST subunits, including KCP2, following SelT depletion is expected to promote a reduction in protein N-glycosylation [40]. To address this issue, we first used a recently developed ER-retained GFP biomarker of N-glycosylation site occupancy whose fluorescence is lost when it is N-glycosylated, due to steric hindrance by the glycan [52] (Fig 5A). Scr and SelT shRNA-transduced AtT20 cells were transfected with ER-GFP and Glyc-ER-GFP, and the GFP fluorescence analyzed after 48 h by confocal microscopy (Fig 5B). Transfection efficiency was assessed using an anti-GFP antibody. Glyc-ER-GFP expressed in scr shRNA-transduced cells did not glow, due to the presence of the N-glycan, but it produced a fluorescent pattern comparable to that seen with ER-GFP in SelT shRNA-transduced cells, indicating that SelT deficiency prevents the N-glycosylation of Glyc-ER-GFP as also shown in Fig 5C. We also explored the effect of SelT depletion on POMC N-glycosylation. Recombinant POMC exists in three different forms, di- and mono-glycosylated and non-glycosylated due to the presence of two N-glycosylation sequons (Fig 5D). Tuni treatment prevented any N-glycosylation to yield only the non-glycosylated POMC isoform. SelT depletion using two different SelT guides for CRISPR Cas9-mediated SelT gene editing led to a decrease in the ratio of glycosylated to total POMC, compared to control conditions (Fig 4E), indicating that POMC N-glycosylation is altered in cells where SelT gene was disrupted. These results show that SelT participate to the N-glycosylation of endogenous glycoproteins. The nature of its substrates is still unclear but several observations indicate that SelT could specifically participate to the N-glycosylation of proteins harboring disulfide bridges. Indeed, SelT expression persists in cells which produce glycoprotein hormones with disulfide bonds, like adult pancreatic insulin- and somatostatin-producing cells, but not in glucagon-producing cells [16], suggesting that it may participate to the N-glycosylation of acceptor sites present in cysteine-rich protein domains before disulfide bond formation, in the same way as MagT1/IAP and TUSC33/N33 present in the B-type OST complex [48].

In conclusion, our data revealed that SelT is essential for ER homeostasis and signaling in order to ensure appropriate hormone production and secretion. They identify for the first time SelT as a subunit of the STT3A-containing OST complex, which is necessary to maintain the integrity of this OST isoform and thereby to achieve N-glycosylation, a key process for endocrine activity [53] and whose deficiency is at the origin of a family of diseases referred to as congenital disorders of glycosylation (CDG) associated with hormonal disturbances [54]. Noteworthy, unicellular eukaryotes lack selenoproteins and selenoprotein synthesis machinery and have no KCP2 homologue that could be identified by sequence similarity. It has been proposed that the role of KCP2 in the A-type OST complex is related to the complexity of N-glycosylation in multicellular eukaryotes [41], a notion that is further supported by this study showing the existence of a particular SelT-containing OST devoted to N-glycosylation in endocrine cells.

Materials and Methods

Cell culture

Mouse corticotroph cells (AtT20), obtained from ATCC, were grown in Dulbecco's modified Eagle's medium (DMEM) (Gibco, Cergy-Pontoise, France) supplemented with 5% heat-inactivated fetal bovine serum (Sigma, Saint Quentin Fallavier, France) and 100 U/ml penicillin, 100 μg/ml streptomycin in a humidified atmosphere of 5% CO_2, 95% air at 37°C. When treated with small hairpin RNA (shRNA), AtT20 cells were maintained in the same medium supplemented with 1 μg/ml of puromycin. ER stress was induced by 100 mM of DTT or 1 μg/ml Tuni for 24 h. In CRISPR Cas9 experiments, Tuni (1 μg/ml) was added in the cell culture medium 24 h after electroporation in order to inhibit N-glycosylation. For pulse-chased experiments with NHK-GFP, cycloheximide was used at 50 μg/ml.

Plasmid constructs

Mouse SelT cDNA comprising the SECIS sequence was amplified from AtT20 cells using forward and reverse primers (Table EV1) and cloned into a pGEM-T vector (Promega, Charbonnières, France). Site-directed mutagenesis was conducted by using the QuikChange® II XL Site-Directed Mutagenesis Kit (Agilent technologies, Les Ulis, France) and specific primers (Table EV1) designed to remove the SelT shRNA recognition sequence or modify the Cys-X-X-Sec active site to Cys-X-X-Cys, Cys-X-X-Ser, Ser-X-X-Cys, and Ser-X-X-Ser. A Myc-SelT variant was also constructed using the QuickChange II XL Site-Directed Mutagenesis Kit to delete the transmembrane helices. Mutants were subsequently cloned in the pCMV-tag5 vector (Agilent Technologies, Les Ulis, France). Nucleotide sequence of all constructs was verified by DNA sequencing.

Immunohistochemistry

Adult mice (male) were anesthetized with pentobarbital and perfused transcardially with 4% paraformaldehyde (PFA) in phosphate-buffered saline (PBS), pH 7.5. The pituitaries were removed and post-fixed in the same solution overnight at 4°C, cryoprotected in 15 and 30% of sucrose, and cut into 14-μm sections. A saturation step (1 h at room temperature) was performed with 1% normal goat serum diluted in a PBS solution containing 1% BSA and 0.3% Triton X-100, prior to overnight incubation with primary antibodies at 4°C. Immunocytochemistry was carried out on AtT20 cells cultured in 12-well plates for 48 h and fixed in 4% PFA. A detailed description of primary antibodies is provided in Table EV2. Alexa-conjugated antibodies (Invitrogen, Cergy-Pontoise, France) including goat anti-rabbit (1:300), goat anti-guinea pig (1:300), goat anti-mouse (1:300) were used as secondary antibodies. Nuclei were stained with 1 μg/ml 4′,6-diamino-2-phenylindole (DAPI; Sigma-Aldrich) in PBS for 2 min. Tissue sections and cells were examined with a Leica SP2 upright confocal laser scanning microscope (DMRAX-UV) equipped with the Acousto-Optico Beam Splitter system (Leica) on the Cell Imaging Platform of Normandy (PRIMACEN, Rouen).

Electron microscope immunohistochemistry

Electron microscopy studies were performed at the Bordeaux Imaging Center, a Core facility of the national infrastructure "France BioImaging" (ANR-10-INBS-04 FranceBioImaging). Adult, male Wistar rats were deeply anesthetized with pentobarbital and then intra-aortically perfused with physiological saline followed by 4% PFA and 0.25% glutaraldehyde in 0.1 M phosphate buffer (PB) for 15 min. Pituitary was removed and immersed in 4% PFA for an additional 2 h, then rinsed in PB overnight at 4°C. The adenohypophysis was cut in 100-μm sagittal slices with a VT 1200S vibratome (Leica). These slices were pre-incubated in 0.1 M Tris–HCl, 0.15 M NaCl and 0.05% Tween T20 (TNT) supplemented with 1% BSA and 1% glycine for 30 min at room temperature. Slices were then treated with the labmade rabbit anti-SelT antibody diluted 1:400 in TNT buffer containing 1% BSA overnight at 4°C then rinsed three times for 10 min in the same buffer. They were incubated with anti-rabbit F(ab')2 coupled with 1.4-nm gold particles (1:100; Aurion) in the same buffer for 2 h at room temperature. After rinsing and further fixation with 1% glutaraldehyde in PB for 10 min, slices were washed three times in water. Gold particles were silver-enhanced in a dark room using the HQ silver enhancement kit (Nanoprobes) for 5 min at room temperature, washed four times in water, then post-fixed with 1% osmium tetroxide for 1 h in PB, dehydrated with ethanol, and flat-embedded in epon. After polymerization, ultra-thin sections perpendicular to the thickness of the vibratome slice were obtained with a Leica UCT ultramicrotome, eventually contrasted with uranyl acetate and lead citrate, and finally observed with an H7650 Hitachi electron microscope. Control slices were submitted to the same treatment except primary antibody.

Yeast split-ubiquitin two-hybrid analysis

Yeast split-ubiquitin two-hybrid screening was performed by Hybrigenics Services (Paris, France). The coding sequence of rat SelT (GenBank accession number gi: 66393088) was PCR-amplified. It was cloned into pBT3-N plasmid in frame with the C-terminus of ubiquitin (Cub) coupled with the artificial transcription factor LexA-VP16 (LexA-VP16-Cub-SelT), or into pBT3-STE in frame with the STE2 leader sequence at the N-terminus and ubiquitin (Cub) coupled with the artificial transcription factor LexA-VP16 (STE2-SelT-Cub-N-LexA-VP16) at the C-terminus. The constructs were checked by sequencing the entire insert. Functional assays were performed to determine the best construct to use for the screen. The proper localization of the bait into the membrane was tested with known membranes proteins. The construct pBT3-STE was used as a bait to screen a dT-primed Mouse Embryo d 11 NubG-x (cDNA library constructed into pPR3-N). The prey proteins were expressed as a fusion to the N-terminal half of ubiquitin (NubG-x). Up to 59 million clones (15-fold the complexity of the library) were screened using a mating approach with NMY32ΔGal4 (mata) and HGX13 (Y187 ade2-101::loxP-kanMX-loxP, matα) yeast strains as previously described (Fromont-Racine *et al*, 1997). Twenty His+ colonies were selected on a medium lacking tryptophan, leucine, and histidine and supplemented with 100 mM 3-aminotriazole to handle bait autoactivation. The prey fragments of the positive clones were amplified by PCR and sequenced at their 5′ junctions. The resulting sequences were used to identify the corresponding interacting proteins in the GenBank database (NCBI) using a fully automated procedure.

Real-time polymerase chain reaction

Total RNA from AtT20 cells was isolated using the NucleoSpin RNA II kit (Macherey-Nagel, Hoert, France), and one μg of RNA was reverse transcribed using the ImPromIITM Reverse-Transcription system (Promega) in the presence of random primers. Relative expression of the various genes was quantified by real-time PCR using SYBR Green PCR Master Mix (Applied Biosystems, Courtaboeuf, France) and 300 nM of the appropriate primers (Table EV1) in an ABI prism 7900HT apparatus (Life Technologies, Villebon sur Yvette, France). Glyceraldehyde-3-phosphate dehydrogenase (GAPDH) was used as an internal control for normalization, and results were expressed as $2-\Delta(\Delta Ct)$ as described by the manufacturer.

SelT knockdown

SelT silencing in AtT20 cells was carried out with a shRNA (Table EV1). A mouse SelT shRNA oligonucleotide was designed (TATCTCCCTCAACCAATTTAT), and a scr shRNA not complementary to any mouse sequence was used as a control. SelT and scr shRNAs were cloned into the lentiviral vector pVIRHD/EP containing a puromycin resistance gene. Constructs were verified by sequencing. In order to produce the lentivirus, HEK-293T cells were cotransfected with the lentiviral vector along with packaging (pCMV-dR8.74) and envelope (pMD2.G) plasmids. The conditioned medium containing the viral particles was collected 2, 3, and 4 days after transfection, centrifuged for 1 h at 500 g at 4°C, supplemented with 8 μg/ml of polybrene, and added for overnight incubation to freshly plated ATt20 cells for infection. Two days after transduction, infected AtT20 cells were selected in 1 μg/ml of puromycin. Knockdown efficiency was determined by Western blot analysis.

CRISPR Cas9

SelT gene invalidation was performed using Cas9-mediated genome editing via non-homologous end joining (NHEJ). Two SelT sgRNA target sequences (Guide #1: 5′-TAAAGATGCAGTACGCCACC-3′; Guide #2: 5′-TCTTGCTGGGCACGCCGCCC-3′) were designed using the CRISPR Design tool hosted by the Massachusetts Institute of Technology (http://crispr.mit.edu) to minimize potential off target effects. Oligos encoding the targeting sequence were annealed and ligated into the pSpCas9(BB)-2A-Puro V2.0 [55] vector digested with BbsI (New England Biolabs). AtT20 (10^6 cells) were electroporated using the Amaxa Nucleofactor system "R" (Lonza, Basel, Switzerland) with 7.5 μg of the CRISPR/Cas9 plasmid, or cotransfected with 5 μg CRISPR/Cas9 plasmid and 5 μg pFLAG-CMV-1 (Sigma Aldrich) expression vector containing the mouse POMC cDNA (positions 204-833; GenBank accession number NM_001278584). POMC expression and SelT expression were analyzed by Western blot 48 h after electroporation.

Preparation of microsomes

Microsomes from AtT20 cells were prepared as described [56]. Briefly, confluent AtT20 cells cultured on two 500-cm^2 plates were collected, washed twice with PBS, and treated 5–10 min on ice with

an ice-cold lysis buffer composed of 10 mM 3-(N-Morpholino) propanesulfonic acid (MOPS) pH 7.5, 0.5 mM $MgCl_2$ and complete protease inhibitor cocktail (Roche Diagnostics, Meylan, France). The lysate was transferred in a Dounce tissue grinder for a 20-stroke homogenization and centrifuged at 10,500 *g* for 15 min at 4°C, after addition of 5.6 ml of solution containing 0.5 M sucrose, 10 mM MOPS pH 7.5, 20 mM NaCl, 100 mM KCl, and 1 mM DTT. The supernatant was centrifuged first at 8,800 *g* for 20 min at 4°C and then at 100,000 *g* for 1 h at 4°C. After resuspension of the microsomal pellet in the same solution, another 100,000 *g* centrifugation for 1 h at 4°C was performed. The resulting pellet was dissociated in a solution composed of 10 mM MOPS pH 7.5, 250 mM sucrose, 10 mM NaCl, 50 m KCl, and 0.5 mM DTT. Protein concentration was assayed using the Bradford method. Fractions of the microsomal preparation were shock frozen and stored at −80°C before use.

Western blot

AtT20 cells were homogenized with Cell Lysis Buffer containing 50 mM HEPES pH 7.6, 150 mM NaCl, 5 mM EDTA, 20 mM NaF, 2 mM Na_3VO_4, supplemented with a protease inhibitor cocktail (Roche Diagnostics). The lysates were cleared by centrifugation at 14,000 *g* for 10 min at 4°C. Proteins were quantified using the Bradford method (Bio-Rad, Marnes-la-Coquette France), separated by SDS–PAGE on 12% polyacrylamide gels, and transferred onto nitrocellulose sheets (GE Healthcare, Velizy-Villacoublay, France). Membranes were blocked for 1 h at room temperature in 5% non-fat dry milk in PBS. Nitrocellulose blots were subsequently incubated overnight at 4°C with primary antibodies (Table EV2). Thereafter, blots were incubated for 1 h with the secondary antibody conjugated to horseradish peroxidase (1:2,000). Immunoreactive bands were visualized by detection of peroxidase activity by chemiluminescence (clarity Western ECL substrate, Bio-Rad). Quantitative analysis of immunoreactivity was performed with Bio-Rad ChemiDoc illumination system using the Image Lab software (Bio-Rad).

Co-immunoprecipitation

AtT20 cells were homogenized at 4°C for 10 min with lysis buffer containing 50 mM Tris–HCl pH 7.5, 150 mM NaCl, 1% Nonidet P-40, 0.5% sodium deoxycholate supplemented with a protease inhibitor cocktail (Sigma-Aldrich). The lysates were cleared by centrifugation at 14,000 *g* for 10 min at 4°C. Co-immunoprecipitations were performed by incubating 2 mg of lysate at 4°C overnight in the presence of 5 μg of a specific antibody and 25 μl of PureProteome Protein G magnetic beads (Millipore, Molsheim, France). Beads were then washed three times with PBS-Tween buffer and denatured with 1× Laemmli buffer at 95°C for 5 min. Samples were analyzed by SDS–PAGE and Western blotting.

ACTH assay

Adrenocorticotropic hormone concentrations were determined using ACTH (Rat, Mouse)-EIA kit (Phoenix, Strasbourg, France) according to the manufacturer's instructions. Briefly, cells were cultured in serum-free DMEM medium with 100 nM of CRF for 24 h. Culture media were collected and used to measure secreted ACTH levels. ACTH content was measured after cell lysis. Total ACTH was calculated by adding secreted and intracellular ACTH.

Cell viability

AtT20 cells were plated at a density of 10^4 cells per well in 96-well plates and incubated overnight. On the following day, cells were treated with ER stressors and incubated for an additional 24 h. Cell viability was measured using the CellTiter-Blue Cell Viability Assay kit (Promega) according to the manufacturer's instructions. Fluorescence measurement was performed using the microplate reader Flexstation3 TECAN3 (Molecular Devices, Saint-Grégoire, France). For SelT rescue experiments, SelT cDNA constructs in pCMV were electroporated in stably SelT shRNA-expressing cells using the Amaxa Nucleofactor system (Lonza, Basel, Switzerland). Viability was measured 24 h later as described above. The empty pCMV vector was used to assess the rescue specificity.

Data analysis

Values are given as the mean ± SEM of at least three independent experiments. Western blot data are representative of a typical experiment repeated three times or more. Statistical analysis was performed by *t*-test or one and two-way ANOVA tests using the GraphPad prism software. Differences were considered significant when *P*-value was < 0.05.

Expanded View for this article is available online.

Acknowledgements
We thank Drs M. Courel (CNRS-UMR7622, Paris), G. Garrel (UMR8251, Paris), and F. Foulquier (CNRS, UMR 8576, Lille) for helpful advices and discussions; Mélina Petrel and Sabrina Lacomme (Bordeaux Imaging Center, Bordeaux) for the preparation of electron microscopy samples; Drs N. Hosokawa (Institute for Frontier Medical Sciences, Kyoto), H. Freeze (Sanford-Burnham Medical Research Institute, La Jolla), and M. Darmon (Inserm U894, Paris) for the NHK-GFP plasmid, the Gly-ER-GFP and ER-GFP constructs, and the dsRed plasmid, respectively. Anti-ACTH, anti-prolactin, anti-GH, anti-TSH, and anti-FSH antibodies were obtained from Dr A. F. Parlow, (NHPP, Harbor-UCLA Medical Center, Torrance, CA). This work was supported by Inserm (U1239), the Conseil Régional de Haute-Normandie, the Université de Rouen-Normandie, and the Interreg program TC2N.

Author contributions
IL and YA designed the experiments. AH, DC, HA, AC, CBur, CBuc, CJ, LG, ML, PL, YA, and IL performed the experiments and analyzed the data. AH, IL, and YA wrote the manuscript.

Conflict of interest
The authors declare that they have no conflict of interest.

References

1. Brocker MJ, Ho JM, Church GM, Soll D, O'Donoghue P (2014) Recoding the genetic code with selenocysteine. *Angew Chem Int Ed Engl* 53: 319 – 323
2. Papp LV, Lu J, Holmgren A, Khanna KK (2007) From selenium to selenoproteins: synthesis, identity, and their role in human health. *Antioxid Redox Signal* 9: 775 – 806

3. Hatfield DL, Tsuji PA, Carlson BA, Gladyshev VN (2014) Selenium and selenocysteine: roles in cancer, health, and development. *Trends Biochem Sci* 39: 112 – 120
4. Labunskyy VM, Hatfield DL, Gladyshev VN (2014) Selenoproteins: molecular pathways and physiological roles. *Physiol Rev* 94: 739 – 777
5. Dikiy A, Novoselov SV, Fomenko DE, Sengupta A, Carlson BA, Cerny RL, Ginalski K, Grishin NV, Hatfield DL, Gladyshev VN (2007) SelT, SelW, SelH, and Rdx12: genomics and molecular insights into the functions of selenoproteins of a novel thioredoxin-like family. *Biochemistry* 46: 6871 – 6882
6. Kryukov GV, Castellano S, Novoselov SV, Lobanov AV, Zehtab O, Guigo R, Gladyshev VN (2003) Characterization of mammalian selenoproteomes. *Science* 300: 1439 – 1443
7. Hawkes WC, Alkan Z (2010) Regulation of redox signaling by selenoproteins. *Biol Trace Elem Res* 134: 235 – 251
8. Shchedrina VA, Zhang Y, Labunskyy VM, Hatfield DL, Gladyshev VN (2010) Structure-function relations, physiological roles, and evolution of mammalian ER-resident selenoproteins. *Antioxid Redox Signal* 12: 839 – 849
9. Steinbrenner H, Speckmann B, Klotz LO (2016) Selenoproteins: antioxidant selenoenzymes and beyond. *Arch Biochem Biophys* 595: 113 – 119
10. Downey CM, Horton CR, Carlson BA, Parsons TE, Hatfield DL, Hallgrimsson B, Jirik FR (2009) Osteo-chondroprogenitor-specific deletion of the selenocysteine tRNA gene, Trsp, leads to chondronecrosis and abnormal skeletal development: a putative model for Kashin-Beck disease. *PLoS Genet* 5: e1000616
11. Rayman MP (2009) Selenoproteins and human health: insights from epidemiological data. *Biochim Biophys Acta* 1790: 1533 – 1540
12. Shrimali RK, Irons RD, Carlson BA, Sano Y, Gladyshev VN, Park JM, Hatfield DL (2008) Selenoproteins mediate T cell immunity through an antioxidant mechanism. *J Biol Chem* 283: 20181 – 20185
13. Bellinger FP, Raman AV, Reeves MA, Berry MJ (2009) Regulation and function of selenoproteins in human disease. *Biochem J* 422: 11 – 22
14. Grumolato L, Ghzili H, Montero-Hadjadje M, Gasman S, Lesage J, Tanguy Y, Galas L, Ait-Ali D, Leprince J, Guerineau NC *et al* (2008) Selenoprotein T is a PACAP-regulated gene involved in intracellular Ca^{2+} mobilization and neuroendocrine secretion. *FASEB J* 22: 1756 – 1768
15. Boukhzar L, Hamieh A, Cartier D, Tanguy Y, Alsharif I, Castex M, Arabo A, Hajji SE, Bonnet JJ, Errami M *et al* (2016) Selenoprotein T exerts an essential oxidoreductase activity that protects dopaminergic neurons in mouse models of Parkinson's disease. *Antioxid Redox Signal* 24: 557 – 574
16. Prevost G, Arabo A, Jian L, Quelennec E, Cartier D, Hassan S, Falluel-Morel A, Tanguy Y, Gargani S, Lihrmann I *et al* (2013) The PACAP-regulated gene selenoprotein T is abundantly expressed in mouse and human beta-cells and its targeted inactivation impairs glucose tolerance. *Endocrinology* 154: 3796 – 3806
17. Tanguy Y, Falluel-Morel A, Arthaud S, Boukhzar L, Manecka DL, Chagraoui A, Prevost G, Elias S, Dorval-Coiffec I, Lesage J *et al* (2011) The PACAP-regulated gene selenoprotein T is highly induced in nervous, endocrine, and metabolic tissues during ontogenetic and regenerative processes. *Endocrinology* 152: 4322 – 4335
18. Jurynec MJ, Xia R, Mackrill JJ, Gunther D, Crawford T, Flanigan KM, Abramson JJ, Howard MT, Grunwald DJ (2008) Selenoprotein N is required for ryanodine receptor calcium release channel activity in human and zebrafish muscle. *Proc Natl Acad Sci USA* 105: 12485 – 12490
19. Reeves MA, Bellinger FP, Berry MJ (2010) The neuroprotective functions of selenoprotein M and its role in cytosolic calcium regulation. *Antioxid Redox Signal* 12: 809 – 818
20. Zhu X, Gleiberman AS, Rosenfeld MG (2007) Molecular physiology of pituitary development: signaling and transcriptional networks. *Physiol Rev* 87: 933 – 963
21. Sengupta A, Carlson BA, Labunskyy VM, Gladyshev VN, Hatfield DL (2009) Selenoprotein T deficiency alters cell adhesion and elevates selenoprotein W expression in murine fibroblast cells. *Biochem Cell Biol* 87: 953 – 961
22. Amodio G, Renna M, Paladino S, Venturi C, Tacchetti C, Moltedo O, Franceschelli S, Mallardo M, Bonatti S, Remondelli P (2009) Endoplasmic reticulum stress reduces the export from the ER and alters the architecture of post-ER compartments. *Int J Biochem Cell Biol* 41: 2511 – 2521
23. Hiramatsu N, Joseph VT, Lin JH (2011) Monitoring and manipulating mammalian unfolded protein response. *Methods Enzymol* 491: 183 – 198
24. Brewer JW (2014) Regulatory crosstalk within the mammalian unfolded protein response. *Cell Mol Life Sci* 71: 1067 – 1079
25. Volchuk A, Ron D (2010) The endoplasmic reticulum stress response in the pancreatic beta-cell. *Diabetes Obes Metab* 12(Suppl 2): 48 – 57
26. Hetz C (2012) The unfolded protein response: controlling cell fate decisions under ER stress and beyond. *Nat Rev Mol Cell Biol* 13: 89 – 102
27. Gass JN, Gifford NM, Brewer JW (2002) Activation of an unfolded protein response during differentiation of antibody-secreting B cells. *J Biol Chem* 277: 49047 – 49054
28. Lipson KL, Fonseca SG, Ishigaki S, Nguyen LX, Foss E, Bortell R, Rossini AA, Urano F (2006) Regulation of insulin biosynthesis in pancreatic beta cells by an endoplasmic reticulum-resident protein kinase IRE1. *Cell Metab* 4: 245 – 254
29. Li J, Ni M, Lee B, Barron E, Hinton DR, Lee AS (2008) The unfolded protein response regulator GRP78/BiP is required for endoplasmic reticulum integrity and stress-induced autophagy in mammalian cells. *Cell Death Differ* 15: 1460 – 1471
30. Wang M, Ye R, Barron E, Baumeister P, Mao C, Luo S, Fu Y, Luo B, Dubeau L, Hinton DR *et al* (2010) Essential role of the unfolded protein response regulator GRP78/BiP in protection from neuronal apoptosis. *Cell Death Differ* 17: 488 – 498
31. Gracia-Navarro F, Malagon MM, Castano JP, Garcia-Navarro S, Sanchez-Hormigo A, Luque RM, Peinado JR, Delgado E (2002) Secretory plasticity of pituitary cells: a mechanism of hormonal regulation. *Arch Physiol Biochem* 110: 106 – 112
32. Holl RW, Thorner MO, Mandell GL, Sullivan JA, Sinha YN, Leong DA (1988) Spontaneous oscillations of intracellular calcium and growth hormone secretion. *J Biol Chem* 263: 9682 – 9685
33. Cao SS, Kaufman RJ (2014) Endoplasmic reticulum stress and oxidative stress in cell fate decision and human disease. *Antioxid Redox Signal* 21: 396 – 413
34. Hetz C, Mollereau B (2014) Disturbance of endoplasmic reticulum proteostasis in neurodegenerative diseases. *Nat Rev Neurosci* 15: 233 – 249
35. Hosokawa N, Wada I, Hasegawa K, Yorihuzi T, Tremblay LO, Herscovics A, Nagata K (2001) A novel ER alpha-mannosidase-like protein accelerates ER-associated degradation. *EMBO Rep* 2: 415 – 422
36. Liu J, Rozovsky S (2015) Membrane-bound selenoproteins. *Antioxid Redox Signal* 23: 795 – 813
37. Fredericks GJ, Hoffmann FW, Rose AH, Osterheld HJ, Hess FM, Mercier F, Hoffmann PR (2014) Stable expression and function of the inositol 1,4,5-triphosphate receptor requires palmitoylation by a DHHC6/selenoprotein K complex. *Proc Natl Acad Sci USA* 111: 16478 – 16483

38. Lee JH, Park KJ, Jang JK, Jeon YH, Ko KY, Kwon JH, Lee SR, Kim IY (2015) Selenoprotein S-dependent Selenoprotein K binding to p97(VCP) protein is essential for endoplasmic reticulum-associated degradation. *J Biol Chem* 290: 29941 – 29952
39. Shchedrina VA, Everley RA, Zhang Y, Gygi SP, Hatfield DL, Gladyshev VN (2011) Selenoprotein K binds multiprotein complexes and is involved in the regulation of endoplasmic reticulum homeostasis. *J Biol Chem* 286: 42937 – 42948
40. Roboti P, High S (2012) The oligosaccharyltransferase subunits OST48, DAD1 and KCP2 function as ubiquitous and selective modulators of mammalian N-glycosylation. *J Cell Sci* 125: 3474 – 3484
41. Roboti P, High S (2012) Keratinocyte-associated protein 2 is a bona fide subunit of the mammalian oligosaccharyltransferase. *J Cell Sci* 125: 220 – 232
42. Shibatani T, David LL, McCormack AL, Frueh K, Skach WR (2005) Proteomic analysis of mammalian oligosaccharyltransferase reveals multiple subcomplexes that contain Sec61, TRAP, and two potential new subunits. *Biochemistry* 44: 5982 – 5992
43. Bonkobara M, Das A, Takao J, Cruz PD, Ariizumi K (2003) Identification of novel genes for secreted and membrane-anchored proteins in human keratinocytes. *Br J Dermatol* 148: 654 – 664
44. Moremen KW, Tiemeyer M, Nairn AV (2012) Vertebrate protein glycosylation: diversity, synthesis and function. *Nat Rev Mol Cell Biol* 13: 448 – 462
45. Aebi M, Bernasconi R, Clerc S, Molinari M (2010) N-glycan structures: recognition and processing in the ER. *Trends Biochem Sci* 35: 74 – 82
46. Ruiz-Canada C, Kelleher DJ, Gilmore R (2009) Cotranslational and post-translational N-glycosylation of polypeptides by distinct mammalian OST isoforms. *Cell* 136: 272 – 283
47. Shrimal S, Cherepanova NA, Gilmore R (2015) Cotranslational and post-translocational N-glycosylation of proteins in the endoplasmic reticulum. *Semin Cell Dev Biol* 41: 71 – 78
48. Kelleher DJ, Gilmore R (2006) An evolving view of the eukaryotic oligosaccharyltransferase. *Glycobiology* 16: 47R – 62R
49. Kelleher DJ, Karaoglu D, Mandon EC, Gilmore R (2003) Oligosaccharyltransferase isoforms that contain different catalytic STT3 subunits have distinct enzymatic properties. *Mol Cell* 12: 101 – 111
50. Dumax-Vorzet A, Roboti P, High S (2013) OST4 is a subunit of the mammalian oligosaccharyltransferase required for efficient N-glycosylation. *J Cell Sci* 126: 2595 – 2606
51. Sanjay A, Fu J, Kreibich G (1998) DAD1 is required for the function and the structural integrity of the oligosaccharyltransferase complex. *J Biol Chem* 273: 26094 – 26099
52. Losfeld ME, Soncin F, Ng BG, Singec I, Freeze HH (2012) A sensitive green fluorescent protein biomarker of N-glycosylation site occupancy. *FASEB J* 26: 4210 – 4217
53. Ikegami K, Liao XH, Hoshino Y, Ono H, Ota W, Ito Y, Nishiwaki-Ohkawa T, Sato C, Kitajima K, Iigo M *et al* (2014) Tissue-specific posttranslational modification allows functional targeting of thyrotropin. *Cell Rep* 9: 801 – 810
54. Grunewald S (2007) Congenital disorders of glycosylation: rapidly enlarging group of (neuro)metabolic disorders. *Early Hum Dev* 83: 825 – 830
55. Ran FA, Hsu PD, Wright J, Agarwala V, Scott DA, Zhang F (2013) Genome engineering using the CRISPR-Cas9 system. *Nat Protoc* 8: 2281 – 2308
56. Legeza B, Balazs Z, Nashev LG, Odermatt A (2013) The microsomal enzyme 17beta-hydroxysteroid dehydrogenase 3 faces the cytoplasm and uses NADPH generated by glucose-6-phosphate dehydrogenase. *Endocrinology* 154: 205 – 213

